

Constraints on nDGP gravity from SPT galaxy clusters with DES and HST weak-lensing mass calibration and from Planck PR4 CMB anisotropies

S. M. L. Vogt,^{1,2,3,*} S. Bocquet,¹ C. T. Davies,¹ J. J. Mohr,^{1,4} F. Schmidt,³ C.-Z. Ruan,⁵ B. Li,⁶
C. Hernández-Aguayo,³ S. Grandis,⁷ L. E. Bleem,^{8,9} M. Klein,^{1,4} M. Aguena,^{10,11} S. Allam,¹²
F. Andrade-Oliveira,¹³ D. Bacon,¹⁴ D. Brooks,¹⁵ R. Camilleri,¹⁶ A. Carnero Rosell,^{17,11,18} J. Carretero,¹⁹
M. Costanzi,^{20,10,21} L. N. da Costa,¹¹ M. E. da Silva Pereira,²² J. De Vicente,²³ P. Doel,¹⁵ J. García-Bellido,²⁴
P. Giles,²⁵ D. Gruen,²⁶ G. Gutierrez,¹² S. R. Hinton,¹⁶ D. L. Hollowood,²⁷ D. J. James,²⁸ K. Kuehn,^{29,30} S. Lee,³¹
J. L. Marshall,³² J. Mena-Fernández,³³ F. Menanteau,^{34,35} R. Miquel,^{36,19} J. Myles,³⁷ A. A. Plazas Malagón,^{38,39}
A. Porredon,^{23,40} J. Prat,⁴¹ C. L. Reichardt,⁴² A. K. Romer,²⁵ E. Sanchez,²³ I. Sevilla-Noarbe,²³ M. Smith,⁴³
M. Soares-Santos,⁴⁴ E. Suchyta,⁴⁵ M. E. C. Swanson,³⁴ C. To,⁴⁶ V. Vikram,⁴⁷ and N. Weaverdyck^{48,49}

(the SPT and DES Collaborations)

¹University Observatory, LMU Faculty of Physics, Scheinerstr. 1, 81679 Munich, Germany

²Excellence Cluster Origins, Boltzmannstr. 2, 85748 Garching, Germany

³Max Planck Institute for Astrophysics, Karl-Schwarzschild-Str. 1, 85748 Garching, Germany

⁴Max Planck Institute for Extraterrestrial Physics, Giessenbachstr. 2, 85748 Garching, Germany

⁵Institute of Theoretical Astrophysics, University of Oslo, 0315 Oslo, Norway

⁶Institute for Computational Cosmology, Department of Physics,
Durham University, South Road, Durham DH1 3LE, UK

⁷Universität Innsbruck, Institut für Astro- und Teilchenphysik, Technikerstr. 25/8, 6020 Innsbruck, Austria

⁸High-Energy Physics Division, Argonne National Laboratory,
9700 South Cass Avenue, Lemont, IL 60439, USA

⁹Kavli Institute for Cosmological Physics, University of Chicago,
5640 South Ellis Avenue, Chicago, IL 60637, USA

¹⁰INAF-Osservatorio Astronomico di Trieste, via G. B. Tiepolo 11, I-34143 Trieste, Italy

¹¹Laboratório Interinstitucional de e-Astronomia - LIneA,
Av. Pastor Martin Luther King Jr, 126 Del Castilho,
Nova América Offices, Torre 3000/sala 817 CEP: 20765-000, Brazil

¹²Fermi National Accelerator Laboratory, P. O. Box 500, Batavia, IL 60510, USA

¹³Physik-Institut, University of Zürich, Winterthurerstrasse 190, CH-8057 Zürich, Switzerland

¹⁴Institute of Cosmology and Gravitation, University of Portsmouth, Portsmouth, PO1 3FX, UK

¹⁵Department of Physics & Astronomy, University College London, Gower Street, London, WC1E 6BT, UK

¹⁶School of Mathematics and Physics, University of Queensland, Brisbane, QLD 4072, Australia

¹⁷Instituto de Astrofísica de Canarias, E-38205 La Laguna, Tenerife, Spain

¹⁸Universidad de La Laguna, Dpto. Astrofísica, E-38206 La Laguna, Tenerife, Spain

¹⁹Institut de Física d'Altes Energies (IFAE), The Barcelona Institute of Science and Technology,
Campus UAB, 08193 Bellaterra (Barcelona) Spain

²⁰Astronomy Unit, Department of Physics, University of Trieste, via Tiepolo 11, I-34131 Trieste, Italy

²¹Institute for Fundamental Physics of the Universe, Via Beirut 2, 34014 Trieste, Italy

²²Hamburger Sternwarte, Universität Hamburg, Gojenbergsweg 112, 21029 Hamburg, Germany

²³Centro de Investigaciones Energéticas, Medioambientales y Tecnológicas (CIEMAT), Madrid, Spain

²⁴Instituto de Física Teórica UAM/CSIC, Universidad Autónoma de Madrid, 28049 Madrid, Spain

²⁵Department of Physics and Astronomy, Pevensey Building, University of Sussex, Brighton, BN1 9QH, UK

²⁶University Observatory, LMU Faculty of Physics, Scheinerstr. 1, 81679 Munich, Germany

²⁷Santa Cruz Institute for Particle Physics, Santa Cruz, CA 95064, USA

²⁸Center for Astrophysics | Harvard & Smithsonian, 60 Garden Street, Cambridge, MA 02138, USA

²⁹Australian Astronomical Optics, Macquarie University, North Ryde, NSW 2113, Australia

³⁰Lowell Observatory, 1400 Mars Hill Rd, Flagstaff, AZ 86001, USA

³¹Jet Propulsion Laboratory, California Institute of Technology,
4800 Oak Grove Dr., Pasadena, CA 91109, USA

³²George P. and Cynthia Woods Mitchell Institute for Fundamental Physics and Astronomy,
and Department of Physics and Astronomy, Texas A&M University, College Station, TX 77843, USA

³³Université Grenoble Alpes, CNRS, LPSC-IN2P3, 38000 Grenoble, France

³⁴Center for Astrophysical Surveys, National Center for Supercomputing
Applications, 1205 West Clark St., Urbana, IL 61801, USA

³⁵Department of Astronomy, University of Illinois at Urbana-Champaign, 1002 W. Green Street, Urbana, IL 61801, USA

³⁶Institució Catalana de Recerca i Estudis Avançats, E-08010 Barcelona, Spain

³⁷Department of Astrophysical Sciences, Princeton University, Peyton Hall, Princeton, NJ 08544, USA

³⁸Kavli Institute for Particle Astrophysics & Cosmology,

P. O. Box 2450, Stanford University, Stanford, CA 94305, USA

³⁹SLAC National Accelerator Laboratory, Menlo Park, CA 94025, USA

⁴⁰*Ruhr University Bochum, Faculty of Physics and Astronomy, Astronomical Institute,
German Centre for Cosmological Lensing, 44780 Bochum, Germany*

⁴¹*Nordita, KTH Royal Institute of Technology and Stockholm University,
Hannes Alfvéns väg 12, SE-10691 Stockholm, Sweden*

⁴²*School of Physics, University of Melbourne, Parkville, VIC 3010, Australia*

⁴³*Physics Department, Lancaster University, Lancaster, LA1 4YB, UK*

⁴⁴*Physik-Institut, University of Zürich, Winterthurerstrasse 190, CH-8057 Zürich, Switzerland*

⁴⁵*Computer Science and Mathematics Division, Oak Ridge National Laboratory, Oak Ridge, TN 37831*

⁴⁶*Department of Astronomy and Astrophysics, University of Chicago, Chicago, IL 60637, USA*

⁴⁷*Argonne National Laboratory, 9700 S. Cass Avenue, Lemont, IL 60439, USA*

⁴⁸*Berkeley Center for Cosmological Physics, Department of Physics,
University of California, Berkeley, CA 94720, US*

⁴⁹*Lawrence Berkeley National Laboratory, 1 Cyclotron Road, Berkeley, CA 94720, USA*

We present constraints on the normal branch of the Dvali-Gabadadze-Porrati (nDGP) braneworld gravity model from the abundance of massive galaxy clusters. On scales below the nDGP crossover scale r_c , the nDGP model features an effective gravity-like fifth force that alters the growth of structure, leading to an enhancement of the halo mass function (HMF) on cluster scales. The enhanced cluster abundance allows for constraints on the nDGP model using cluster samples. We employ the SPT cluster sample, selected through the thermal Sunyaev-Zel'dovich effect (tSZE) with the South Pole Telescope (SPT) and with mass calibration using weak-lensing data from the Dark Energy Survey (DES) and the Hubble Space Telescope (HST). The cluster sample contains 1,005 clusters with redshifts $0.25 < z < 1.78$, which are confirmed with the Multi-Component Matched Filter (MCMF) algorithm using optical and near-infrared data. Weak-lensing data from DES and HST enable a robust mass measurement of the cluster sample. We use DES Year 3 data for 688 clusters with redshifts $z < 0.95$, and HST data for 39 clusters with redshifts $0.6 < z < 1.7$. We account for the enhancement in the HMF through a semi-analytic correction factor to the $\nu\Lambda$ CDM HMF derived from the spherical collapse model in the nDGP model. We then further calibrate this model using N -body simulations. In addition, for the first time, we analyze the primary cosmic microwave background (CMB) temperature and polarization anisotropy measurements from Planck PR4 within the nDGP model. We obtain a competitive constraint from the joint analysis of the SPT cluster abundance with the Planck PR4 data, and report an upper bound of $1/\sqrt{H_0 r_c} < 1.41$ at 95 % when assuming a cosmology with massive neutrinos.

I. INTRODUCTION

Understanding the observed accelerated expansion of the Universe remains one of the most fundamental open questions in cosmology [1, 2]. The standard cosmological model, Λ cold dark matter (Λ CDM), assumes gravity follows general relativity (GR) and that the accelerated expansion is sourced through a cosmological constant Λ , which is added to the Einstein-Hilbert action. This corresponds to a dark energy component with constant density that drives the acceleration of the Universe's expansion. An independent test of GR, and thus of our understanding of gravity, can be performed by considering modifications to GR, which are generally obtained from extensions of the Einstein-Hilbert action (for a review, see, e.g., [3–5]).

One widely studied modified gravity model is the Dvali-Gabadadze-Porrati (DGP) braneworld gravity model [6]. In the DGP model, our four-dimensional Universe is embedded in a five-dimensional spacetime, and gravity can leak into the extra dimension on large scales, whereas the other fundamental forces remain four-dimensional. Specifically, this transition happens at the

so-called crossover scale r_c , which serves as an extra parameter in the theory that describes the deviation from GR. On scales larger than r_c gravity becomes five-dimensional. Conversely, GR is recovered if $r_c \rightarrow \infty$. However, the GR limit is nontrivial, and the gravitational dynamics and the growth of cosmic structure are modified even on scales much smaller than r_c . GR is restored only in regions with density much higher than the cosmological mean, via the Vainshtein screening mechanism which arises from non-linearities in the modified Poisson equation [7]. In this work, we focus on the normal branch of the DGP model (nDGP) with a quintessence-like dark energy component tuned to give a background expansion history consistent with Λ CDM [8]. Unlike the self-accelerating branch, the normal branch is stable and theoretically consistent. Due to the screening mechanism, which restores GR locally, as well as the unmodified background expansion, the growth of structure is the most stringent observational test of this scenario.

Modified gravity theories such as nDGP alter the linear and non-linear growth of structure on cosmological scales, making summary statistics of the large-scale structure powerful probes for testing these models. One such measure of the large-scale structure is the abundance of massive galaxy clusters [9, 10], which has been widely used to study standard cosmological models [11–19] as well as modified gravity [20–26] and dark matter models [27, 28].

* s.vogt@physik.lmu.de

To obtain cosmological constraints from the abundance of massive galaxy clusters, we need a link between the cluster observables and the underlying mass of the cluster, which is not a directly observed quantity [29, 30]. To make an inference of the underlying cluster masses, we rely on weak lensing to inform these mass estimates.

In this study, we use the sample of 1,005 galaxy clusters detected with the South Pole Telescope (SPT) [31] via the thermal Sunyaev-Zel'dovich effect (tSZE) [32]. The tSZE is a spectral distortion of the cosmic microwave background (CMB) along the cluster line of sight, which is induced by the inverse Compton scattering of low-energy CMB photons with the high-energy electrons of the hot intracluster medium (ICM). Therefore, the tSZE is a direct tracer of the ICM and the underlying massive galaxy cluster. The tSZE signal is approximately redshift independent, and with sufficient angular resolution and sensitivity, clusters can be detected out to the highest redshifts where they exist. The tSZE enables the construction of a high-purity sample with well-understood completeness. SPT cluster candidates are confirmed using the Multi-Component Matched Filter (MCMF) algorithm [33–35] with optical and near-infrared data from the Dark Energy Survey (DES) [36–38] and the Wide-field Infrared Survey Explorer (WISE) [39].

The relation of the tSZE signal to the underlying mass must be calibrated with external data, as modeling the ICM is challenging. Here, we rely on mass measurements from weak-lensing shear data, for which the relation to the mass is well understood and can therefore be used to empirically calibrate the scaling relations between the cluster observables and the cluster mass. We use weak-lensing data from the DES Year 3 shape catalog for 688 clusters with redshifts $z < 0.95$ [40] and targeted observation from the Hubble Space Telescope (HST) for 39 clusters in the redshift range $0.6 < z < 1.7$ [41–43]. The analysis presented in this work is based on the method developed in [18, 44] (hereafter [SB24b](#), [SB24a](#)).

To account for the impact of nDGP on structure formation, we adopt a halo mass function (HMF) model which accounts for changes in spherical collapse in nDGP relative to GR [8]. The analytical model applied here uses the critical collapse overdensity δ_c and the virial overdensity Δ_{vir} derived from a spherical collapse calculation that incorporates the Vainshtein screening. Furthermore, we calibrate the subsequent semi-analytical HMF model against the BRIDGE N -body simulations [45–47], ensuring accurate predictions for the abundance of collapsed structures in nDGP.

We also perform an nDGP analysis of the primary CMB Planck PR4 data [48] using the linear power spectrum in the nDGP model, which is computed from the linearized growth equation in the nDGP cosmology. We obtain constraints on the nDGP model from Planck PR4 alone, as well as in combination with the SPT cluster dataset. Our results are highly competitive with the constraints on the nDGP model from clustering wedge statistics of the galaxy correlation function and estimated

growth rate values. This was applied to BOSS DR1 with Planck 15 priors on Ω_m and A_s and resulted in the tightest constraint on nDGP so far [49].

This paper is organized as follows. Section II presents the cluster data from SPT and a short summary of the weak-lensing data from DES and HST. The nDGP model, the corresponding HMF, and its calibration with the BRIDGE simulations are outlined in Sec. III. The following Sec. IV describes the analysis methodology, including the scaling relations, weak-lensing model, and the Planck data used in this work. Section V presents the results of this work. We conclude the paper with a summary in Sec. VI.

II. DATA

This section gives a brief summary of the cluster and weak-lensing data used in this work. A detailed description of the data products is presented in [SB24a](#).

A. SPT cluster catalog

The tSZE-selected galaxy cluster sample is created from the SPT-SZ, SPTpol ECS, and SPTpol 500d surveys. The three surveys cover 5,270 deg² of the southern sky [35, 50, 51], largely overlapping with the DES footprint. Cluster candidates are selected based on the tSZE detection significance $\hat{\zeta}$ and confirmed using optical and infrared data, which provide redshift measurements and center positions.

In the 1,327 deg² region that is outside the DES footprint ($\sim 27\%$ of the total area), the candidates are selected by $\hat{\zeta} > 5$ and confirmed by targeted follow-up observations, resulting in a sample of 110 clusters, with a purity $\gtrsim 95\%$ [50, 51].

In the 3,567 deg² region that DES covers, clusters are confirmed using the MCMF tool [33, 34], which also provides cluster redshifts, optical richnesses $\hat{\lambda}$, and center positions. For clusters with $z < 1.1$ we use data from DES and for clusters with $z > 1.1$, WISE data are used. The MCMF tool confirms a cluster if the optical richness is higher than a redshift-dependent richness threshold $\hat{\lambda}_{\text{min}}(z)$ which ensures a constant sample purity $> 98\%$. The selection cut in $\hat{\zeta}$ varies between surveys due to different depths and is given by: $\hat{\zeta} > 4.25$ for SPTpol 500d, $\hat{\zeta} > 4.5$ for SPT-SZ and $\hat{\zeta} > 5$ for SPTpol ECS. This yields 895 confirmed clusters in the DES region [[SB24b](#)].

In total, the sample consists of 1,005 clusters with $z > 0.25$, where the lower redshift cut is employed due to contamination from the atmosphere and primary CMB anisotropies.

B. DES Y3 and HST weak-lensing data

We use (when available) weak-lensing shear profiles measured from the DES Y3 shape catalog [40] for clusters within the overlapping SPT-DES region. The profiles are computed within the radial range $0.5 < r/(h^{-1}\text{Mpc}) < 3.2(1 + z_{\text{cluster}})^{-1}$, where z_{cluster} is the cluster redshift, ensuring the exclusion of the central region and the two-halo regime. These weak-lensing measurements are used for clusters with $z < 0.95$, resulting in a sample of 688 SPT clusters with DES shear data [SB24a]. The redshift cut is based on the median redshift of DES's highest-redshift source bin.

For high-redshift clusters, we supplement the DES weak-lensing dataset with HST observations [41–43]. A total of 39 clusters in the redshift range $0.6 - 1.7$ have HST shear measurements. Further details on the HST dataset and methodology can be found in [41–43, 52–54]. In total 727 of our cluster sample of 1,005 clusters have weak-lensing information.

Our weak-lensing analysis accounts for a wide range of systematic uncertainties, including cluster member contamination, miscentering effects, shear and photometric redshift calibration, halo mass modeling, and the influence of the large-scale structure. A detailed description of the modeling of these uncertainties is provided in SB24a. Although these models were calibrated within the Λ CDM framework, we expect that they remain essentially unchanged in the nDGP model, as significant deviations from GR are already ruled out.

III. nDGP GRAVITY

In this section, we briefly discuss the main aspects of the nDGP gravity model, including the modifications to GR collapse dynamics, and discuss the subsequent difference compared to the GR HMF.

In the DGP gravity model, the four-dimensional space-time (the brane) is embedded in a five-dimensional space-time (the bulk). While all particles are confined to the four-dimensional brane, gravity can propagate along the additional spatial dimension and leak into the five-dimensional bulk on large scales. Based on this assumption, the DGP action is given by [6]

$$S = \int_{\text{brane}} d^4x \sqrt{-g} \left(\frac{R}{16\pi G} + \mathcal{L}_m \right) + \int_{\text{bulk}} d^5x \sqrt{-g^{(5)}} \left(\frac{R^{(5)}}{16\pi G^{(5)}} \right), \quad (1)$$

where g denotes the determinant of the metric tensor $g_{\mu\nu}$, G is the gravitational constant, R is the Ricci scalar in the brane and superscripts (5) denote the quantities in the 5-dimensional bulk. Note that we use natural units with $\hbar = c = 1$. The length scale at which gravity becomes five-dimensional is called the crossover scale, which

is defined as

$$r_c = \frac{1}{2} \frac{G^{(5)}}{G}. \quad (2)$$

From matter domination onward, the modified Friedmann equation is given by [55, 56]

$$H(a) = H_0 \sqrt{\Omega_m a^{-3} + \Omega_{\text{de}}(a) + \Omega_{\text{rc}} \pm \sqrt{\Omega_{\text{rc}}}}. \quad (3)$$

Here H_0 is the expansion rate at redshift 0, Ω_m is the matter density parameter, Ω_{de} is the dark energy density parameter and $\Omega_{\text{rc}} := 1/(4H_0 r_c)$. The different signs represent the two branches of the DGP theory. The self-accelerating branch ($-$ sign, sDGP) results in a late-time accelerating universe even without a dark energy component, i.e. $\Omega_{\text{de}} = 0$. However, sDGP suffers from ghost instabilities [57–59] and is also ruled out by supernova and CMB data [60]. The $+$ sign refers to the normal branch nDGP and requires a dark energy component to yield an accelerating universe. In this paper, we consider the normal branch and tune the density and equation of state of the dark energy such that the background history matches that in Λ CDM, i.e. $H(a) = \sqrt{\Omega_m a^{-3} + \Omega_\Lambda}$ [8, 61]. It is also possible to assume an nDGP scenario without introducing an evolving dark energy component to match the Λ CDM background evolution, i.e. assuming Eq. (3) with $\Omega_{\text{de}} = \Omega_\Lambda$ constant. However, in this scenario, the background evolution is significantly different from Λ CDM, and the constraint on the crossover scale r_c is dominated by geometric probes rather than the growth of structure [56, 62, 63].

If we consider scales smaller than the Horizon, H^{-1} , as well as the crossover scale r_c , which is entirely sufficient for the observables considered here, nDGP can be described as an effective scalar-tensor theory with an extra scalar field, the brane-bending mode φ . This field arises from the ability of the brane to move in the extra dimension and mediates a gravity-like fifth force. Effectively, it contributes to the metric potentials by

$$\nabla^2 \Phi = 4\pi G \delta\rho + \frac{1}{2} \nabla^2 \varphi, \quad (4)$$

$$\nabla^2 \Psi = 4\pi G \delta\rho - \frac{1}{2} \nabla^2 \varphi. \quad (5)$$

In the quasistatic regime, again appropriate on the sub-horizon scales considered here, the equation of motion for the brane bending mode is given by [8]

$$\nabla^2 \varphi + \frac{r_c^2}{3\beta(a)} [(\nabla^2 \varphi)^2 - (\nabla_i \nabla_j \varphi)^2] = \frac{8\pi G}{3\beta(a)} \delta\rho, \quad (6)$$

with the function

$$\beta(a) = 1 + 2H(a)r_c \left(1 + \frac{\dot{H}(a)}{3H^2(a)} \right). \quad (7)$$

From the above equation, if $r_c \rightarrow \infty$ then $\nabla^2 \varphi = 0$ and the equations for the metric potentials, Eqs. (4) and (5), return to their Λ CDM expressions.

In low density regions, we can linearize Eqs. (4) and (5) by neglecting quadratic terms in Eq. (6) and obtain the following relation for the dynamical potential:

$$\nabla^2 \Phi = 4\pi \left(1 + \frac{1}{3\beta}\right) G\delta\rho, \quad (8)$$

$$\nabla^2(\Phi + \Psi) = 4\pi G\delta\rho. \quad (9)$$

Note that the second relation states that the potential combination governing gravitational lensing (null geodesics) is unmodified from GR. From the first relation on the other hand, the linearized growth equation is given by

$$\ddot{\delta} + 2H\dot{\delta} = 4\pi \left(1 + \frac{1}{3\beta}\right) G\delta\rho, \quad (10)$$

which differs from the Λ CDM equation by a factor $1 + \frac{1}{3\beta}$. Because $\beta(a)$ depends only on time, the nDGP linear growth of structure is scale-independent. Thus the nDGP linear matter power spectrum, $P_L^{\text{nDGP}}(k)$, is given by the Λ CDM linear power spectrum with the same initial condition (i.e. same primordial amplitude A_s) rescaled by the ratio of the growth factors squared D^2 derived from Eq. (10).

Tests of gravity on solar system scales report results consistent with GR. Therefore, any deviations from GR must be suppressed on solar system scales [64–66]. In nDGP, the nonlinearities in the field Eq. (6) suppress the fifth force in these dense environments. If $r_c \sim H_0^{-1}$, then the suppression acts in any region with density much higher than the cosmological background. This is known as the Vainshtein screening mechanism [7].

A. Collapse dynamics and the halo mass function

To constrain nDGP gravity with the cluster abundance, we need a model for the nDGP halo mass function (HMF). In this work, we use the Sheth-Tormen HMF [67] adapted for nDGP, which is based on the model presented in Refs. [8, 61]. The Sheth-Tormen HMF is given by

$$\left. \frac{dn}{d\ln M} \right|_{\text{ST}} = -\frac{1}{2} \frac{\bar{\rho}_m}{M_{\text{vir}}} f(\delta_c/\sigma)_{\text{ST}} \frac{d\ln \sigma^2}{d\ln M_{\text{vir}}}. \quad (11)$$

We use the following quantities calculated in the nDGP model: the variance of the linear matter power spectrum, $\sigma^2(M)$, the linearly extrapolated collapse overdensity, δ_c , and the virial overdensity, Δ_{vir} . Note that the Sheth-Tormen HMF uses the virial mass, $M_{\text{vir}} = 4/3\pi\Delta_{\text{vir}}\bar{\rho}R_{\text{vir}}^3$, as a mass definition. Since we are using $M_{200\text{crit}}$, we transform the above HMF to $M_{200\text{crit}}$ by performing a mass rescaling, also propagating the derivative $dM_{200\text{crit}}/dM_{\text{vir}}$ [61]. This model has been shown to agree well with N -body simulations of the nDGP model [8]. As presented at the end of this section, we further calibrate this model with additional N -body simulations to improve its accuracy and utility.

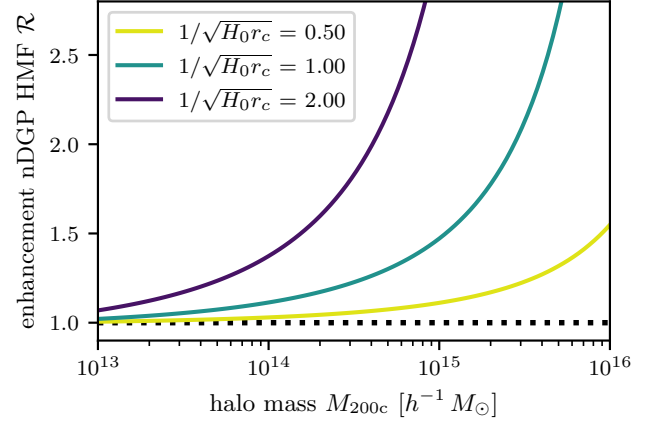


FIG. 1. Enhancement of the nDGP HMF with respect to the corresponding Λ CDM cosmology from Eq. (15) in colored lines for different strengths of the nDGP model at mean cluster sample redshift $z = 0.6$. The enhancement depends on the strength of the nDGP model and grows exponentially with mass. The black dashed line shows the Λ CDM limit with no enhancement, i.e. $\mathcal{R} = 1$.

As described in the previous section, the linear power spectrum in nDGP is the Λ CDM power spectrum rescaled by the growth factor ratio, and thus we have

$$\sigma(M, z) = \sigma^{\Lambda\text{CDM}}(M, z) \frac{D^{\text{nDGP}}(z)}{D^{\Lambda\text{CDM}}(z)}. \quad (12)$$

δ_c is computed from the full equation of motion for the density perturbation in a spherically symmetric setup,

$$\ddot{\delta} + 2H\dot{\delta} - \frac{4}{3} \frac{\dot{\delta}}{1+\delta} = (1+\delta)\nabla^2\Phi. \quad (13)$$

We find the initial overdensity δ_i such that the collapse of a spherical top-hat overdensity occurs at the collapse redshift z_c . δ_c is computed from the linear extrapolation of the initial overdensity δ_i using Eq. (10).

The virial overdensity Δ_{vir} is the mean overdensity of a spherical overdensity with radius R_{vir} with respect to the background density. The virial radius is defined as the radius (after turn-around) that satisfies the virial equation at a specific virial redshift z_{vir} . The density contrast at z_{vir} is then given as $1 + \delta(R_{\text{vir}})$ and is extrapolated to the collapse redshift z_c to define the virial overdensity:

$$\Delta_{\text{vir}} = [1 + \delta(R_{\text{vir}})] \left(\frac{1 + z_{\text{vir}}}{1 + z_c} \right)^3 \quad (14)$$

The three computed quantities are used to calculate the Sheth-Tormen HMF in the nDGP model. In practice, we are not using the Sheth-Tormen HMF directly. Instead, we capture the deviations from the Λ CDM Sheth-Tormen HMF with the same initial conditions by computing the ratio of Sheth-Tormen HMFs in the two models

$$\mathcal{R} = \frac{\left. \frac{dn}{d\ln M} \right|_{\text{ST, nDGP}}}{\left. \frac{dn}{d\ln M} \right|_{\text{ST, } \Lambda\text{CDM}}}. \quad (15)$$

To obtain the HMF in nDGP gravity, we multiply this ratio by a Λ CDM HMF of our choice. This approach has the advantage of being independent of the Sheth-Tormen HMF and can be adapted to use any HMF as a baseline. In this work, we use the Tinker HMF $\frac{dn}{d\ln M}|_{\text{T},\Lambda\text{CDM}}$ [68] as the Λ CDM baseline and thus the nDGP HMF is given by

$$\frac{dn}{d\ln M} = \mathcal{R} \frac{dn}{d\ln M} \Big|_{\text{T},\Lambda\text{CDM}}. \quad (16)$$

Figure 1 shows the ratio predicted by Eq. (15) for different values of the nDGP parameter $1/\sqrt{H_0 r_c}$ at the mean redshift of the cluster sample $z = 0.6$. As expected from the enhanced structure formation, the HMF is increased in nDGP gravity. Moreover, the enhancement depends strongly on mass and shows a significant deviation from Λ CDM for massive halos, which is because the HMF is exponentially sensitive to $\delta_c/\sigma(M)$ at high masses. We account for the effect of massive neutrinos by using the baryonic and cold dark matter only power spectrum in our calculations [69, 70] and refer to a standard cosmology with massive neutrinos as $\nu\Lambda$ CDM.

Since the Sheth-Tormen HMF is a semi-analytical model, we want to compare the results of Eq. (15) to non-linear simulations to validate these models. For this we use the BRIDGE simulations [45–47], which cover a wide range of nDGP cosmologies by varying the parameters Ω_m , h , $S_8^{\Lambda\text{CDM}} = \sigma_8^{\Lambda\text{CDM}} \sqrt{\Omega_m/0.3}$, and $\log(H_0 r_c)$, and with a box length of $L = 500 h^{-1} \text{Mpc}$. In addition to each nDGP simulation, a Λ CDM box was created with the same initial conditions. Note that the simulations use massless neutrinos; therefore, the calibration with these simulations does not account for the effects of massive neutrinos. In total 49 cosmologies plus one fiducial Λ CDM cosmology are simulated, and we use the snapshots at nine evenly distributed redshifts between 0 and 2 to compute the ratio of halo numbers from the nDGP and the Λ CDM boxes, $\mathcal{R}_{\text{BRIDGE}}$. The comparison for four redshifts is shown in Fig. 2, and one sees that the two ratios do not fully agree. Based on the comparison in Fig. 2, we model the bias between the semi-analytical model and the simulations as a constant $q+1$ for each cosmology. We limit the correction to a constant bias, as the shot noise in the simulations precludes us from reliably fitting a more complex fitting function. Fitting the bias q for each cosmology yields a linear trend in $1/\sqrt{H_0 r_c}$ and redshift z . Therefore, we model the correction as follows

$$\frac{\mathcal{R}_{\text{BRIDGE}}}{\mathcal{R}_{\text{SAM}}} = \tilde{q} \left(\frac{1}{\sqrt{H_0 r_c}} - 0.1 \right) (z - 0.8) + 1. \quad (17)$$

Here \tilde{q} is the mean bias, and we choose pivot values in $1/\sqrt{H_0 r_c}$ and z of 0.1 and 0.8, respectively. We separate the dependence on $1/\sqrt{H_0 r_c}$ and z from the bias through the above modeling and obtain a mean bias parameter $\tilde{q} = 0.06$ for the correction function. Applying the above one-parameter correction to the ratio of the semi-analytical model to the simulations reduces the

scatter between the semi-analytical model and the simulations by 26% from 0.0073 to 0.0058. This uncertainty is based on the corrected comparison of the HMF enhancements from the second row of Fig. 2 for each redshift and mass bin, where the scatter is obtained over the 49 simulations. Note that we assume no bias for cosmologies with $1/\sqrt{H_0 r_c} < 0.1$, because the bias should vanish for $1/\sqrt{H_0 r_c} = 0$ as we approach Λ CDM.

To summarize, the full nDGP HMF used in our analysis is given by

$$\begin{aligned} \frac{dn}{d\ln M}(M, z) &= \frac{dn}{d\ln M}(M, z) \Big|_{\text{T}} \mathcal{R} \\ &\times \left[\tilde{q} \left(\frac{1}{\sqrt{H_0 r_c}} - 0.1 \right) (z - 0.8) + 1 \right]. \end{aligned} \quad (18)$$

and we also account for an 8% uncertainty in the amplitude of the HMF based on the scatter from the corrected HMF enhancement.

IV. CLUSTER ANALYSIS METHOD

Our analysis follows the state-of-the-art cluster analysis with weak-lensing informed mass calibration developed for the SPT cluster sample [SB24a]. This chapter briefly summarizes the cluster analysis, and we refer the reader to [SB24a] and [SV24b] for more details.

A. Observable–mass relations

Clusters of galaxies are detected through observables such as the tSZE detection significance and optical richness, with empirical scaling relations connecting these observables to the halo mass e.g., [72, 73]. A connection between the halo observable function and the HMF can be made by calibrating these relations with weak gravitational lensing measurements. This connection allows us to relate observables to the HMF, which is sensitive to cosmology, and provides constraints on cosmological parameters.

The observed tSZE detection significance, $\hat{\zeta}$, is linked to the intrinsic detection significance, ζ following the relation [74]:

$$P(\hat{\zeta}|\zeta) = \mathcal{N} \left(\sqrt{\zeta^2 + 3}, 1 \right), \quad (19)$$

which accounts for observational noise. The mean intrinsic tSZE detection significance, ζ , is linked to the underlying mass and redshift by the following power law:

$$\begin{aligned} \langle \ln \zeta \rangle &= \ln \zeta_0 + \zeta_M \ln \left(\frac{M_{200c}}{3 \times 10^{14} h^{-1} M_\odot} \right) \\ &+ \zeta_z \ln \left(\frac{E(z)}{E(0.6)} \right). \end{aligned} \quad (20)$$

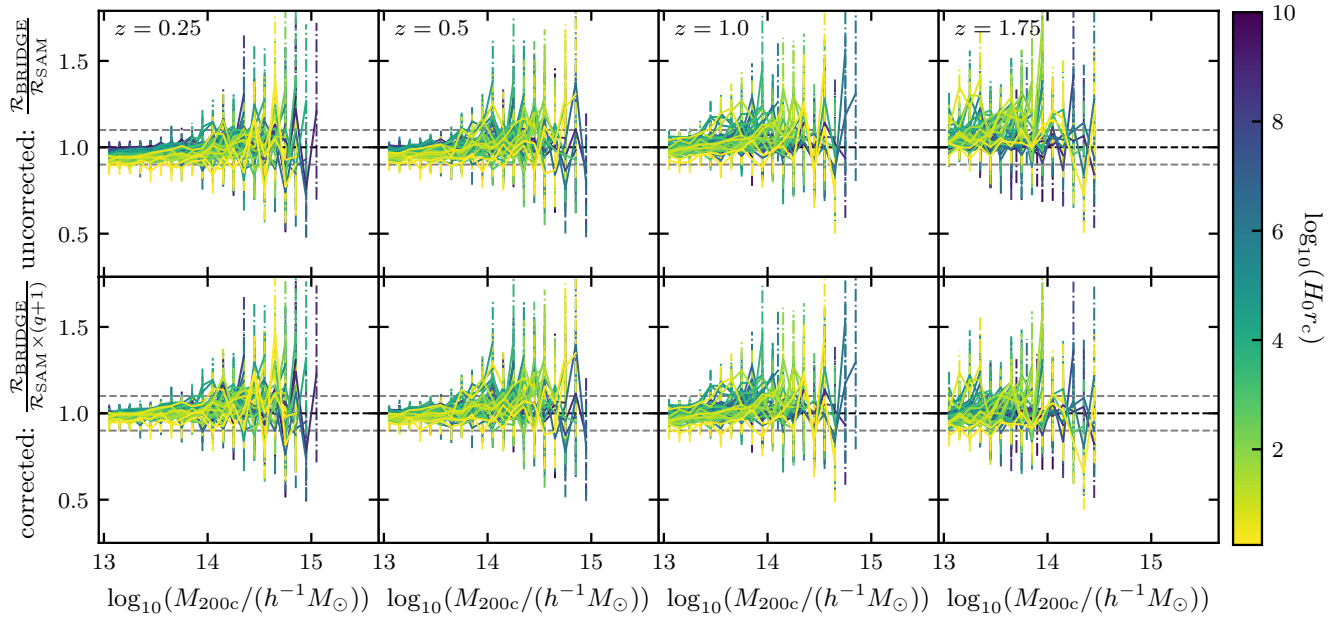


FIG. 2. Comparison between the HMF enhancement predicted by the BRIDGE simulations, $\mathcal{R}_{\text{BRIDGE}}$, and the semi-analytical model, \mathcal{R}_{SAM} , across various redshifts. The data points are color-coded by $\log(H_0 r_{\text{rmc}})$ values. Gray dashed lines indicate $\pm 10\%$ deviation as a visual reference. The top four panels present the uncorrected comparison based on Eq. (15), while the bottom four panels show the results after applying the correction factor from Eq. (17), resulting in improved agreement. Error bars reflect the jackknife covariance estimated from the BRIDGE simulation.

A lognormal intrinsic scatter with variance $\sigma_{\ln \zeta}$ around this mean relation is assumed. To account for variation in survey depth, ζ_0 and ζ_z are rescaled for each SPT field and survey, respectively [35, 50, 51]. The normalization factor γ_{ECS} of ζ_0 for the SPTpol ECS survey is difficult to determine and thus is treated as an additional free parameter in the analysis.

Similarly, the observed richness, $\hat{\lambda}$, relates to the intrinsic richness, λ , through a Gaussian distribution:

$$P(\hat{\lambda}|\lambda) = \mathcal{N}(\lambda, \sqrt{\lambda}). \quad (21)$$

This approximates the Poisson sampling noise in the richness estimation. The mean intrinsic richness follows a power-law dependence on mass and redshift:

$$\begin{aligned} \langle \ln \lambda \rangle = & \ln \lambda_0 + \lambda_M \ln \left(\frac{M_{200c}}{3 \times 10^{14} h^{-1} M_{\odot}} \right) \\ & + \lambda_z \ln \left(\frac{1+z}{1.6} \right). \end{aligned} \quad (22)$$

We assume a lognormal scatter width $\sigma_{\ln \lambda}$ around this relation.

For clusters with $z \leq 1.1$, richness is measured using DES, while for high-redshift ($z > 1.1$) clusters, WISE data are used. As these datasets have different richness measurements, we adopt separate λ -mass relations for DES and WISE clusters [SB24b].

The scaling relation described above enables the translations of the halo observable function in the ζ - λ - z space

to the halo mass functions and allows constraints on cosmological parameters. However, given the lack of information on the priors of these scaling relation parameters and their scatters, we rely on additional observations to calibrate these relations empirically. As the link between the mass of a cluster and the corresponding weak-lensing signal is well understood, using weak-lensing data for this calibration is robust.

B. Cluster weak-lensing model

The model we adopt for the DES weak-lensing data has been studied and described in detail in SB24a and the references therein. Here, we summarize the key aspects of this approach. It is important to note that we assume any modifications arising from nDGP gravity in the mapping from cluster mass to lensing signal to be negligible. While in the nDGP model the lensing signal for a given mass distribution is unmodified from GR, nDGP gravity can still change the halo profiles. However, these modifications have been found to be minor [75]. Note that any variations in the cluster observables $\hat{\zeta}$ and $\hat{\lambda}$ at fixed halo mass are accounted for by the empirical calibration of the observable-mass relations.

The weak-lensing observable is the reduced shear and is related by a projected Navarro-Frenk-White profile

(NFW) [76, 77] to a mass, M_{WL} , by

$$g_t(r, M_{\text{WL}}) = \frac{\Delta\Sigma(r, M_{\text{WL}}) \Sigma_{\text{crit}}^{-1}}{1 - \Sigma(r, M_{\text{WL}}) \Sigma_{\text{crit}}^{-1}}. \quad (23)$$

We refer to the mass inferred from this observable as the weak-lensing mass M_{WL} of the cluster. Since real cluster profiles deviate from a perfect NFW profile, the inferred weak-lensing mass M_{WL} is a biased and noisy estimator of the true cluster mass M_{200c} [78, 79]. To correct for this bias, we adopt a scaling relation between M_{WL} and M_{200c} , with the mean relation given by [80]:

$$\left\langle \ln \left(\frac{M_{\text{WL}}}{M_0} \right) \right\rangle = \ln M_{\text{WL}_0}(z) + M_{\text{WL}_M} \ln \left(\frac{M_{200c}}{M_0} \right). \quad (24)$$

Here $\ln M_{\text{WL}_0}$ is the logarithmic mass bias normalization and M_{WL_M} is the mass trend in this bias at a pivot mass $M_0 = 2 \times 10^{14} h^{-1} M_\odot$. We model the scatter around this relation with a lognormal distribution with a variance given by:

$$\ln \sigma_{\ln \text{WL}}^2 = \ln \sigma_{\ln \text{WL}_0}^2(z) + \sigma_{\ln \text{WL}_M}^2 \ln \left(\frac{M_{200c}}{M_0} \right), \quad (25)$$

where $\ln \sigma_{\ln \text{WL}_0}^2$ is the normalization and $\sigma_{\ln \text{WL}_M}^2$ is the mass trend of the scatter. The parameters defining the mean scaling relation and the scatter are calibrated using hydrodynamical simulations, where the weak-lensing inferred mass is extracted and compared to the corresponding true cluster mass obtained from matched gravity-only simulations across different redshifts [44, 80].

A similar model is applied to the HST dataset. Here, the weak-lensing mass M_{WL} is mapped to the true halo mass with a mean relation [41],

$$\langle \ln M_{\text{WL}} \rangle = \ln M_{\text{WL}_0} + \ln M_{200c}, \quad (26)$$

where $\ln M_{\text{WL}_0}$ is the bias between the true halo and weak-lensing mass. The mean relation scatters around the mean with a Gaussian distribution of width $\sigma_{\ln \text{WL}}$. The two parameters are found on a cluster-by-cluster basis. We refer the reader to the original works for a more detailed explanation of the cluster lensing model employed for the HST dataset [41–43, 54].

C. Cluster Likelihood

Our analysis is based on a Bayesian analysis framework, where we determine the posterior distributions of cosmological and scaling relation parameters through a cluster population model. The likelihood function used in this study follows the methodology from Refs. [SB24b, SB24a]. We assume that a Poisson distribution gives the

multi-observable cluster abundance likelihood:

$$\begin{aligned} \ln \mathcal{L} \left(\{\hat{\zeta}, \hat{\lambda}_i, z_i, \mathbf{g}_{t,i}\}_{i=1}^{N_{\text{cluster}}} | \mathbf{p} \right) = & \\ & \sum_{i=1}^{N_{\text{cluster}}} \ln \frac{d^4 N(\mathbf{p})}{d\hat{\zeta} d\hat{\lambda} d\mathbf{g}_t dz} \Big|_{\hat{\zeta}_i, \hat{\lambda}_i, \mathbf{g}_{t,i}, z_i} \\ & - \int \cdots \int d\hat{\zeta} d\hat{\lambda} d\mathbf{g}_t dz \frac{d^4 N(\mathbf{p})}{d\hat{\zeta} d\hat{\lambda} d\mathbf{g}_t dz} \Theta_s(\hat{\zeta}, \hat{\lambda}, z) \\ & + \text{const.} \end{aligned} \quad (27)$$

where the index i runs over all observed clusters, and $\Theta_s(\hat{\zeta}, \hat{\lambda}, z)$ represents the sample selection function, see Sec. II A. The differential cluster abundance entering the likelihood function is expressed as:

$$\begin{aligned} \frac{d^4 N(\mathbf{p})}{d\hat{\zeta} d\hat{\lambda} d\mathbf{g}_t dz} = & \int d\Omega_s \int \cdots \int dM d\zeta d\lambda dM_{\text{WL}} \\ & P(\hat{\zeta}|\zeta) P(\hat{\lambda}|\lambda) P(\mathbf{g}_t|M_{\text{WL}}, \mathbf{p}) \\ & P(\zeta, \lambda, M_{\text{WL}}|M, z, \mathbf{p}) \\ & \frac{d^2 N(M, z, \mathbf{p})}{dM dV} \frac{d^2 V(z, \mathbf{p})}{dz d\Omega_s}. \end{aligned} \quad (28)$$

Here, Ω_s represents the survey solid angle. The terms $\frac{d^2 N(M, z, \mathbf{p})}{dM dz}$ and $\frac{d^2 V(z, \mathbf{p})}{dz d\Omega_s}$ correspond to the HMF and the differential volume element, respectively. The probabilities $P(\hat{\zeta}|\zeta)$, $P(\hat{\lambda}|\lambda)$, and $P(\mathbf{g}_t|M_{\text{WL}}, \mathbf{p})$ describe the relationships between the observed and intrinsic quantities. The joint probability $P(\zeta, \lambda, M_{\text{WL}}|M, z, \mathbf{p})$ is the multi-observable-mass relation, accounting for potential correlations among the three observables. Our model is described by 23 astrophysical parameters and seven cosmological parameters, denoted by \mathbf{p} .

In the analysis, we use uniform priors for the cosmological parameters Ω_m , $\ln 10^{10} A_s$, $\Omega_\nu h^2$, and $1/\sqrt{H_0 r_c}$ as well as for all scaling relation parameters. We adopt Gaussian priors for the weak-lensing parameters in Eqs. (24)–(26). The cluster abundance does not constrain the cosmological parameters $\Omega_b h^2$, n_s and h , and we apply Gaussian priors on the first two from Planck and a Gaussian prior on the latter of $h \sim \mathcal{N}(0.70, 0.05^2)$. In the joint analysis with Planck, we use uniform priors for these parameters instead.

D. Planck PR4 data and likelihood

Primary CMB data, such as those from the Planck satellite, place tight constraints on standard cosmological parameters and can break degeneracies with modified gravity parameters. Therefore, the combination of the cluster abundance and primary CMB anisotropies can impose competitive constraints on nDGP. In this work, we use the latest Planck PR4 data to achieve such constraints, adopting HiLLiPoP likelihoods for the high- l TT, TE and EE spectra and the LoLLiPoP low- l EE

spectrum likelihood [48]. For the low- l TT spectrum, the original Planck PR3 likelihood is used [81]. The CMB power spectrum in nDGP is derived from the linearized metric potential equations (8) and (9), where the deviations from GR are encoded in the modification functions μ and γ respectively. To compute the nDGP power spectrum, we implemented the two nDGP expressions for μ and γ in the Boltzmann code MGCAMB [82–85].¹

When using primary CMB data from Planck, the results on scale-independent modified gravity models change from Planck PR3 to Planck PR4 [81, 86, 87]. Earlier Planck analysis from Planck 15 [88] and Planck PR3 [81] reported a $\sim 2.1\sigma$ detection of a scale-independent modified gravity model.² This is due to the CMB lensing anomaly [89–91]. This anomaly refers to a systematic effect found in the Planck PR3 data, which prefers a smoother power spectrum at high l than predicted from the standard cosmological model. The tension can be resolved by introducing an empirical lensing parameter A_{lens} , which modifies the amplitude of the CMB lensing effect and is unity for Λ CDM by definition. Allowing A_{lens} to vary improves the fit to the data and gives a value of A_{lens} away from unity at the $2 - 3\sigma$ level. The empirical A_{lens} parameter is degenerate with the modified gravity parameter μ and, if not accounted for, the $A_{\text{lens}} \neq 1$ anomaly can lead to a detection of scale-independent modified gravity in the analyses of Planck 15 and Planck PR3 [81, 87, 92]. Recently, the A_{lens} anomaly was resolved with the LoLLiPoP and HiLLiPoP likelihoods, through more advanced modeling of the systematics [48]. Therefore, we decide to use this latter likelihood combination. A detailed comparison of the nDGP constraints derived from different Planck datasets is provided in Appendix A.

V. RESULTS

In this section, we present the constraints on nDGP gravity from SPT clusters with mass calibration from DES and HST, Planck PR4 and the combination. Note that all reported uncertainties are provided at the 68 % credible level and upper limits at 95 % credibility.

A. nDGP constraint from clusters

Figure 3 shows in red the results from the SPT cluster abundance alone for the four parameters Ω_m , A_s , σ_8 , and $1/\sqrt{H_0 r_c}$. The posterior shows that the nDGP parameter $1/\sqrt{H_0 r_c}$ cannot be meaningfully constrained by this SPT dataset alone. This is mainly due to the degeneracy

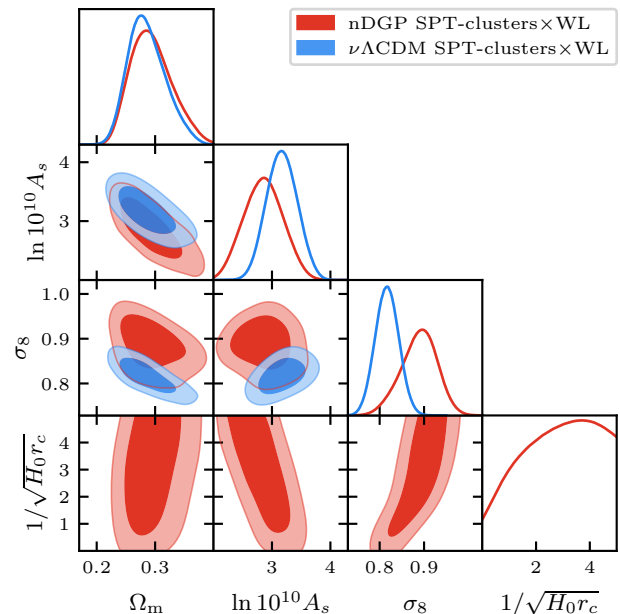


FIG. 3. Posterior distribution on Ω_m , $\log_{10} A_s$, σ_8 and $1/\sqrt{H_0 r_c}$ (68 % and 95 % credible regions) for the nDGP SPT-clusters \times WL analysis in red and for reference the $\nu\Lambda$ CDM analysis from SB24b in blue. The cluster dataset alone cannot meaningfully constrain the nDGP parameter $1/\sqrt{H_0 r_c}$. Compared to the $\nu\Lambda$ CDM analysis, the constraint on Ω_m remains the same while σ_8 (which is computed using the nDGP linear growth equation) is shifted to higher values due to the enhanced growth in nDGP.

between $1/\sqrt{H_0 r_c}$ and the standard cosmological parameters, such as Ω_m and A_s . These degeneracies are visible in the two-dimensional contours of Fig. 3. A negative correlation between A_s and $1/\sqrt{H_0 r_c}$ is visible which accounts for the fact that an increase in the HMF due to modified gravity can be compensated by a lower initial amplitude of fluctuations. Note that σ_8 in our definition includes the modified growth, see Eq. (12), and is a function of both A_s and $1/\sqrt{H_0 r_c}$. Therefore, a positive correlation emerges between $1/\sqrt{H_0 r_c}$ and σ_8 .

Figure 3 also shows the $\nu\Lambda$ CDM baseline analysis of SB24b in blue. In comparison, the uncertainty in Ω_m remains almost unchanged and increases only by 7 % in the nDGP analysis. In contrast, the uncertainty in σ_8 increases by 58 %, and its posterior shifts to higher values. This shift arises because the SPT clusters constrain the amplitude of matter fluctuations at an effective redshift characteristic of the sample, here $z \sim 0.6$, and on an effective physical scale that does not correspond exactly to $8 h^{-1}$ Mpc. Because the growth history in nDGP depends on $1/\sqrt{H_0 r_c}$ and is different than in Λ CDM, mapping this cluster constrained amplitude to $\sigma_8(z=0)$ leads to a higher inferred present-day value of σ_8 . The shift to lower values of A_s , discussed above, reflects the compensation of the HMF enhancement induced by modified gravity.

¹ <https://github.com/sfu-cosmo/MGCAMB>

² Note that the Planck analyses adopted a different parametrization of the modification function μ and γ , but this remains valid for nDGP gravity as shown in Appendix A.

In summary, the current SPT cluster dataset does not provide sufficient information to constrain all three parameters simultaneously, particularly the nDGP parameter. However, ongoing galaxy cluster surveys such as SPT-3G [93] and the Simons Observatory [94] will significantly improve the sensitivity to cosmological parameters and offer the potential to constrain modified gravity models without relying on additional datasets [26].

In Fig. 6 in Appendix B, we present the full posterior distributions, comparing the nDGP and $\nu\Lambda$ CDM analyses. The scaling relation parameters of the ζ -mass and λ -mass relations show good agreement with the $\nu\Lambda$ CDM baseline result. As expected, the uncertainties on these parameters are slightly larger in the nDGP analysis due to the additional degree of freedom introduced by the modified gravity model. Moreover, we do not observe any significant degeneracies between the nDGP and scaling relation parameters.

B. nDGP constraint from Planck PR4

In this work, we also present the first constraints on the nDGP gravity model from the primary CMB Planck data. We show the posterior distribution of Ω_m , σ_8 and $1/\sqrt{H_0 r_c}$ from Planck PR4 alone in Fig. 4 in green. We report an upper limit on the nDGP parameter $1/\sqrt{H_0 r_c}$ from Planck PR4 of

$$1/\sqrt{H_0 r_c} < 1.62 \quad (95\% \text{ limit}). \quad (29)$$

This result is consistent with zero at 95 % credibility and thus we find no significant deviation from GR. The obtained value of σ_8 from the nDGP analysis is higher than from the $\nu\Lambda$ CDM analysis due to the enhanced structure formation coming from the additional fifth force (see Sec. III). A positive correlation between σ_8 and $1/\sqrt{H_0 r_c}$ is seen because the CMB primarily constraints the primordial amplitude A_s , and, for fixed A_s , σ_8 depends on $1/\sqrt{H_0 r_c}$ as shown in Eq. (12).

The constraints on the nDGP model from the primary CMB Planck data depend on the underlying Planck dataset and likelihood. In Appendix A, we present results considering different Planck datasets and analysis choices. In the main analysis, we rely on the most recent and up-to-date Planck PR4 release from Ref. [48].

C. nDGP constraint from SPT-clusters \times WL+PR4

Finally, we combine both of the above considered datasets. For this, we multiply the primary CMB Planck PR4 likelihood with the SPT-cluster \times WL dataset likelihood, which is meaningful when the two posteriors are statistically consistent, with the additional assumption that there is no correlation between the two datasets. As shown in Fig. 4, the combination tightens the constraints on Ω_m , σ_8 and $1/\sqrt{H_0 r_c}$. While the tightening of the

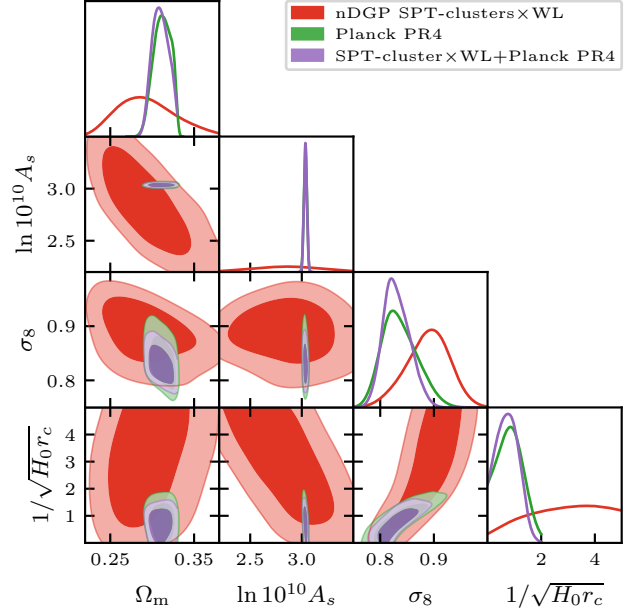


FIG. 4. Posterior distribution on Ω_m , A_s , σ_8 and $1/\sqrt{H_0 r_c}$ (68 % and 95 % credible regions) for the nDGP SPT-cluster \times WL analysis in red, Planck PR4 in green and the combination in purple. The joint analysis places a competitive constraint on the nDGP parameter $1/\sqrt{H_0 r_c} < 1.41$ at 95 % credibility.

constraint on Ω_m is mild, the improvement on $1/\sqrt{H_0 r_c}$ and σ_8 is much larger. From the combination, we get an upper limit on the nDGP parameter of

$$1/\sqrt{H_0 r_c} < 1.41 \quad (95\% \text{ limit}), \quad (30)$$

which is 15 % tighter than the Planck PR4 only results. The constraints on the other cosmological parameters can be found in Tab. I. In comparing our results to the literature, a few considerations should be taken into account. First, a meaningful comparison can only be made if the nDGP model studied in the related work also assumes a Λ CDM expansion history [see discussion after Eq. (3)]. Therefore, we restrict our comparison to Refs. [49, 95]. In addition, our analysis allows the total neutrino mass to vary, whereas Refs. [49, 95] assume massless neutrinos. This difference prevents a direct comparison of the results. To address this, we also perform an analysis with zero neutrino mass and obtain a tighter constraint of $1/\sqrt{H_0 r_c} < 1.14$, which we use for the comparison below. Ref. [95] uses measurements of the monopole and quadrupole of the two-point correlation function of the LRG sample from SDSS II DR7 and found $r_c > 340$ Mpc, which translates to $1/\sqrt{H_0 r_c} < 3.6$ at 95 % credibility [95]. Ref. [49] reported the current tightest constraints on nDGP gravity with a Λ CDM background evolution by using clustering wedges statistics of the galaxy correlation function measured from BOSS DR1 with Planck 15 priors on Ω_m and A_s . There, the authors reported $1/(H_0 r_c) < 0.97$ which translates to

TABLE I. Constraints on the cosmological parameters Ω_m , σ_8 , $\sum m_\nu$ and $1/\sqrt{H_0 r_c}$ for the three datasets used in this work (mean and 68% credible intervals, or 95% limit). The nDGP parameter $1/\sqrt{H_0 r_c}$ and the total neutrinos mass $\sum m_\nu$ are not a meaningful constraint by the SPT-cluster \times WL dataset alone (missing entries (...) in the table), and we only quote the constraints from Planck PR4 and the combination for these parameters. For comparison to other literature results, we also quote in the last row the result from the combination with massless neutrinos.

Dataset	Ω_m	σ_8	$\sum m_\nu$ [eV]	$1/\sqrt{H_0 r_c}$
SPT-clusters \times WL	0.294 ± 0.035	0.889 ± 0.040
Planck PR4	0.312 ± 0.010	0.837 ± 0.033	< 0.26	< 1.62
SPT-clusters \times WL + Planck PR4	0.3098 ± 0.0095	0.831 ± 0.025	< 0.24	< 1.41
SPT-clusters \times WL + Planck PR4 ($\sum m_\nu = 0$ eV)	0.2984 ± 0.0064	$0.842^{+0.027}_{-0.012}$	0	< 1.14

$1/\sqrt{H_0 r_c} < 0.99$ at 95% credibility. In comparison, we see that our constraint (when assuming massless neutrinos) is three times tighter in $1/\sqrt{H_0 r_c}$ than the one reported in Ref. [95] and is of the same level (17% less tight) as the most stringent constraint from Ref. [49]. Importantly, our analysis goes beyond simply incorporating additional priors from Planck as done by Ref. [49], whereas we perform a self-consistent joint analysis of the cluster dataset and the primary CMB data from Planck using the explicit likelihoods for both datasets.

VI. SUMMARY

In this paper, we present a cosmological analysis of the nDGP gravity model using the abundance of massive galaxy clusters detected with SPT with weak-lensing mass information from DES and HST and in combination with Planck PR4. The cluster sample consists of 1,005 clusters with redshifts $z > 0.25$, selected from the SPT-SZ, SPTpol ECS and SPTpol 500d surveys [35, 50, 51] and confirmed with the MCMF algorithm [33, 34] (in the DES footprint) and targeted follow-up observations. We use weak-lensing tangential shear profiles for the simultaneous weak-lensing mass calibration from DES for 688 clusters with $z < 0.95$ [40] and HST measurements for 39 SPT clusters with higher redshifts $0.6 - 1.6$ [41–43]. The analysis framework used here is based on the state-of-the-art cluster analysis presented in [SB24b, SB24a].

The nDGP gravity model alters the structure growth on cosmological scales by introducing an effective gravity-like fifth force [6, 8, 61], thereby affecting and enhancing the abundance of massive galaxy clusters compared to the standard cosmological model. Therefore, the HMF is modified, and we use a semi-analytical approach, where we rescale the $\nu\Lambda$ CDM HMF with an enhancement factor to account for the increased clustering due to the fifth force [8, 61]. This rescaling involves the spherical collapse quantities computed in the nDGP gravity model, including the critical overdensity δ_c and the virial overdensity Δ_{vir} .

To validate the semi-analytical model we compare it against the BRIDGE simulations [45–47], a set of 49 N -body simulations for nDGP gravity with different values of the cosmological parameters Ω_m , h , $S_8^{\text{GR}} =$

$\sigma_8^{\Lambda\text{CDM}} \sqrt{\Omega_m/0.3}$, and $\log(H_0 r_c)$. We find good agreement for nDGP model realizations close to GR (i.e. $\log(H_0 r_c)$ large or $1/\sqrt{H_0 r_c}$ close to zero). A bias is noticeable for larger deviations from GR between the simulations and the semi-analytical HMF. We model this bias as a mass-independent factor that depends on the nDGP parameter $1/\sqrt{H_0 r_c}$ and redshift z , and correct our semi-analytical HMF accordingly. This correction reduces the overall scatter between the semi-analytical model and the simulations by 26%.

Using the nDGP HMF within a Bayesian analysis framework for the SPT cluster sample allows us to constrain nDGP gravity with the abundance of massive galaxy clusters. We find that SPT clusters alone cannot place a meaningful constraint on the nDGP gravity parameter $1/\sqrt{H_0 r_c}$. This is due to the degeneracies between $1/\sqrt{H_0 r_c}$ and the two standard cosmological parameters Ω_m , σ_8 . We conclude that an external probe is needed to break degeneracies and obtain a competitive constraint on the nDGP modified gravity model with the SPT clusters. Moreover, all standard cosmological parameters and the scaling relation parameters are consistent with the $\nu\Lambda$ CDM analysis of Ref. [SB24b], as expected since our analysis does not show a statistically significant hint for the nDGP model.

We use primary CMB data from Planck PR4 [48], which benefits from improved systematic modeling over previous releases, particularly with respect to the CMB lensing anomaly which is degenerate with the modified gravity parameter [81, 87, 89–92]. Using Planck PR4 data alone, we obtain an upper bound of $1/\sqrt{H_0 r_c} < 1.62$ at 95% credibility.

Combining Planck PR4 with the SPT cluster data tightens the constraint to $1/\sqrt{H_0 r_c} < 1.41$ (95% credible level). This result is competitive with the currently most stringent constraint from Ref. [49]. We also find that this combination improves the constraint on σ_8 , while the constraint on Ω_m is dominated by Planck (see Fig. 4 and Tab. I).

Upcoming galaxy cluster surveys such as SPT-3G [93] or the Simons Observatory [94] will provide much larger cluster samples. Paired with next-generation weak-lensing data from Euclid [96] and the Legacy Survey of Space and Time (LSST) [97] at the Vera C. Rubin Observatory these cluster samples will lead to tight con-

straints on standard cosmology and potential extensions to gravity [26, 27]. Another avenue to tighten the constraints on modified gravity theories would be to incorporate ground-based CMB data from SPT and ACT in cluster-based analyses [98, 99].

ACKNOWLEDGMENTS

This research was supported by 1) the Excellence Cluster ORIGINS, which is funded by the Deutsche Forschungsgemeinschaft (DFG, German Research Foundation) under Germany’s Excellence Strategy - EXC-2094-390783311, by 2) the Max Planck Society Faculty Fellowship program at MPE, and by 3) the Ludwig-Maximilians-Universität in Munich.

BL is funded by UK STFC through Consolidate Grant ST/X001075/1

The South Pole Telescope program is supported by the National Science Foundation (NSF) through awards OPP-1852617 and OPP-2332483. Partial support is also provided by the Kavli Institute of Cosmological Physics at the University of Chicago. Argonne National Laboratory’s work was supported by the U.S. Department of Energy, Office of High Energy Physics, under contract DE-AC02-06CH11357.

Funding for the DES Projects has been provided by the U.S. Department of Energy, the U.S. National Science Foundation, the Ministry of Science and Education of Spain, the Science and Technology Facilities Council of the United Kingdom, the Higher Education Funding Council for England, the National Center for Supercomputing Applications at the University of Illinois at Urbana-Champaign, the Kavli Institute of Cosmological Physics at the University of Chicago, the Center for Cosmology and Astro-Particle Physics at the Ohio State University, the Mitchell Institute for Fundamental Physics and Astronomy at Texas A&M University, Financiadora de Estudos e Projetos, Fundação Carlos Chagas Filho de Amparo à Pesquisa do Estado do Rio de Janeiro, Conselho Nacional de Desenvolvimento Científico e Tecnológico and the Ministério da Ciência, Tecnologia e Inovação, the Deutsche Forschungsgemeinschaft and the Collaborating Institutions in the Dark Energy Survey.

The Collaborating Institutions are Argonne National Laboratory, the University of California at Santa Cruz, the University of Cambridge, Centro de Investigaciones Energéticas, Medioambientales y Tecnológicas-Madrid, the University of Chicago, University College London, the DES-Brazil Consortium, the University of Edinburgh, the Eidgenössische Technische Hochschule (ETH) Zürich, Fermi National Accelerator Laboratory, the University of Illinois at Urbana-Champaign, the Institut de Ciències de l’Espai (IEEC/CSIC), the Institut de Física d’Altes Energies, Lawrence Berkeley National Laboratory, the Ludwig-Maximilians-Universität München and the associated Excellence Cluster Origins, the University of Michigan, NSF’s NOIRLab, the University of Notting-

ham, The Ohio State University, the University of Pennsylvania, the University of Portsmouth, SLAC National Accelerator Laboratory, Stanford University, the University of Sussex, Texas A&M University, and the OzDES Membership Consortium.

Based in part on observations at Cerro Tololo Inter-American Observatory at NSF’s NOIRLab (NOIRLab Prop. ID 2012B-0001; PI: J. Frieman), which is managed by the Association of Universities for Research in Astronomy (AURA) under a cooperative agreement with the National Science Foundation.

The DES data management system is supported by the National Science Foundation under Grant Numbers AST-1138766 and AST-1536171. The DES participants from Spanish institutions are partially supported by MICINN under grants ESP2017-89838, PGC2018-094773, PGC2018-102021, SEV-2016-0588, SEV-2016-0597, and MDM-2015-0509, some of which include ERDF funds from the European Union. IFAE is partially funded by the CERCA program of the Generalitat de Catalunya. Research leading to these results has received funding from the European Research Council under the European Union’s Seventh Framework Program (FP7/2007-2013) including ERC grant agreements 240672, 291329, and 306478. We acknowledge support from the Brazilian Instituto Nacional de Ciência e Tecnologia (INCT) do e-Universo (CNPq grant 465376/2014-2).

This work is based on observations made with the NASA/ESA *Hubble Space Telescope*, using imaging data from the SPT follow-up GO programs 12246 (PI: C. Stubbs), 12477 (PI: F. W. High), 13412 (PI: T. Schrabback), 14252 (PI: V. Strazzullo), 14352 (PI: J. Hlavacek-Larrondo), and 14677 (PI: T. Schrabback). STScI is operated by the Association of Universities for Research in Astronomy, Inc. under NASA contract NAS 5-26555. It is also based on observations made with ESO Telescopes at the La Silla Paranal Observatory under programs 086.A-0741 (PI: Bazin), 088.A-0796 (PI: Bazin), 088.A-0889 (PI: Mohr), 089.A-0824 (PI: Mohr), 0100.A-0204 (PI: Schrabback), 0100.A-0217 (PI: Hernández-Martín), 0101.A-0694 (PI: Zohren), and 0102.A-0189 (PI: Zohren). It is also based on observations obtained at the Gemini Observatory, which is operated by the Association of Universities for Research in Astronomy, Inc., under a cooperative agreement with the NSF on behalf of the Gemini partnership: the National Science Foundation (United States), National Research Council (Canada), CONICYT (Chile), Ministerio de Ciencia, Tecnología e Innovación Productiva (Argentina), Ministério da Ciência, Tecnologia e Inovação (Brazil), and Korea Astronomy and Space Science Institute (Republic of Korea), under programs 2014B-0338 and 2016B-0176 (PI: B. Benson).

This manuscript has been authored by Fermi Research Alliance, LLC under Contract No. DE-AC02-07CH11359 with the U.S. Department of Energy, Office of Science, Office of High Energy Physics.

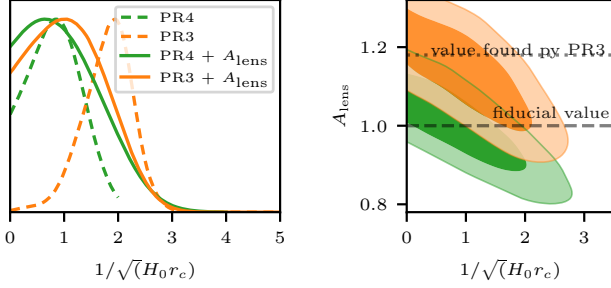


FIG. 5. *Left:* 1D posterior distribution for the nDGP parameter $1/\sqrt{H_0 r_c}$ for the different Planck datasets with and without varying the lensing parameter A_{lens} in solid and dashed lines, respectively. Planck PR3 indicated a 3.7σ detection on the nDGP model. This detection goes away if A_{lens} is varied as well as with the Planck PR4 analysis pipeline. *Right:* Posterior distribution for $1/\sqrt{H_0 r_c}$ and A_{lens} for Planck PR3 and Planck PR4. Both datasets show a negative correlation between the two parameters, as both have a smoothing effect on the high l CMB power spectrum. For reference, the black dashed lines show the fiducial value of A_{lens} and the black dotted line shows the recovered value of the Planck PR3 analysis.

Appendix A: Planck and modified gravity

As mentioned in Sec. IV D, the constraint on nDGP gravity from Planck primary CMB depends on the choice of the Planck dataset and analysis pipeline. Earlier Planck analysis, such as Planck PR3, found a $\sim 2.1\sigma$ detection of scale-independent modified gravity away from Λ CDM [81]. In this work, a different scale-independent modified gravity parametrization is used and we include massive neutrinos in our analysis. We re-analyzed the Planck PR3 data with an nDGP gravity model and found similar results with an even higher detection of the nDGP parameters, which is 3.7σ away from $\nu\Lambda$ CDM as seen in Fig. 5 in blue. This detection is related to the lensing anomaly found in the earlier Planck analyses [81, 88]. The lensing anomaly reflects the systematic effect that the Planck data prefer a larger lensing-induced smoothing of the CMB power spectrum at high l than predicted from a GR cosmology. To investigate this tension, an artificial lensing amplitude parameter A_{lens} was introduced, which allows for more smoothing, and the theoretical prediction in Λ CDM is $A_{\text{lens}} = 1$ [89]. In Planck PR3 the data preferred $A_{\text{lens}} > 1$ at the 3σ level in the Λ CDM

analysis, leading to a tension between the data and the standard cosmological model.

Because modified gravity models enhance lensing and thus increase lensing-induced smoothing, the effect on the CMB power spectrum is the same as having $A_{\text{lens}} > 1$ in Λ CDM and $\nu\Lambda$ CDM cosmologies. Therefore, earlier Planck analyses preferred modified gravity parameters away from the GR limit. Suppose A_{lens} is a free parameter in the analysis with a modified gravity model. In that case, the constraints on the modified gravity parameters are consistent with GR, because one accounts for the correlation between the two parameters [81, 86, 87]. In the case of nDGP gravity, with the Planck PR3 data and pipeline we find a result consistent with $\nu\Lambda$ CDM at the 1.7σ level. The shift in the posterior with and without varying A_{lens} can be seen in Fig. 5 on the left side for Planck PR3 in solid and dashed orange lines, respectively.

The recent Planck PR4 analysis resolved the lensing anomaly, where $A_{\text{lens}} = 1.039 \pm 0.052$ was reported [48]. Therefore, analyzing scale-independent modified gravity models with Planck PR4 data and pipeline leads to consistent results with GR without varying the lensing parameter A_{lens} [86, 87]. In this paper, we present the constraint from Planck PR4 on the nDGP model and report $1/\sqrt{H_0 r_c} > 1.45$ at 95 % credibility. If we also vary A_{lens} we find a weaker constraint of $1/\sqrt{H_0 r_c} > 2.28$ at 95 % credible interval as seen in Fig. 5 on the left side in green. The constraint is weaker because A_{lens} already accounts for smoothing the CMB power spectrum at high l .

This section explains that modified gravity and the lensing parameter A_{lens} have the same effect on the high- l CMB power spectrum. Therefore, we expect a degeneracy between the two parameters. The right side of Fig. 5 shows the 2-D posterior of $1/\sqrt{H_0 r_c}$ and A_{lens} , and as expected, a negative correlation can be seen. This is related to the fact that $A_{\text{lens}} > 1$ and $1/\sqrt{H_0 r_c} > 0$ enhance both the smoothing of the CMB lensing, and thus when we account for the smoothing from nDGP, A_{lens} is reduced.

Appendix B: Full posterior results

We present the posterior distribution for all parameters from our cluster analysis in Fig. 6. For comparison, we added the results from the $\nu\Lambda$ CDM analysis.

-
- [1] S. Perlmutter, G. Aldering, G. Goldhaber, R. A. Knop, P. Nugent, P. G. Castro, S. Deustua, S. Fabbro, A. Goobar, D. E. Groom, et al., *Astrophys. J.* **517**, 565 (1999), [arXiv:astro-ph/9812133](#).
 - [2] A. G. Riess, A. V. Filippenko, P. Challis, A. Clocchiatti, A. Diercks, P. M. Garnavich, R. L. Gilliland, C. J. Hogan, S. Jha, R. P. Kirshner, et al., *ApJ* **116**, 1009 (1998),

[arXiv:astro-ph/9805201](#).

- [3] A. Joyce, L. Lombriser, and F. Schmidt, *Annual Review of Nuclear and Particle Science* **66**, 95 (2016), [arXiv:1601.06133](#).
- [4] K. Koyama, *International Journal of Modern Physics D* **27**, 1848001 (2018).

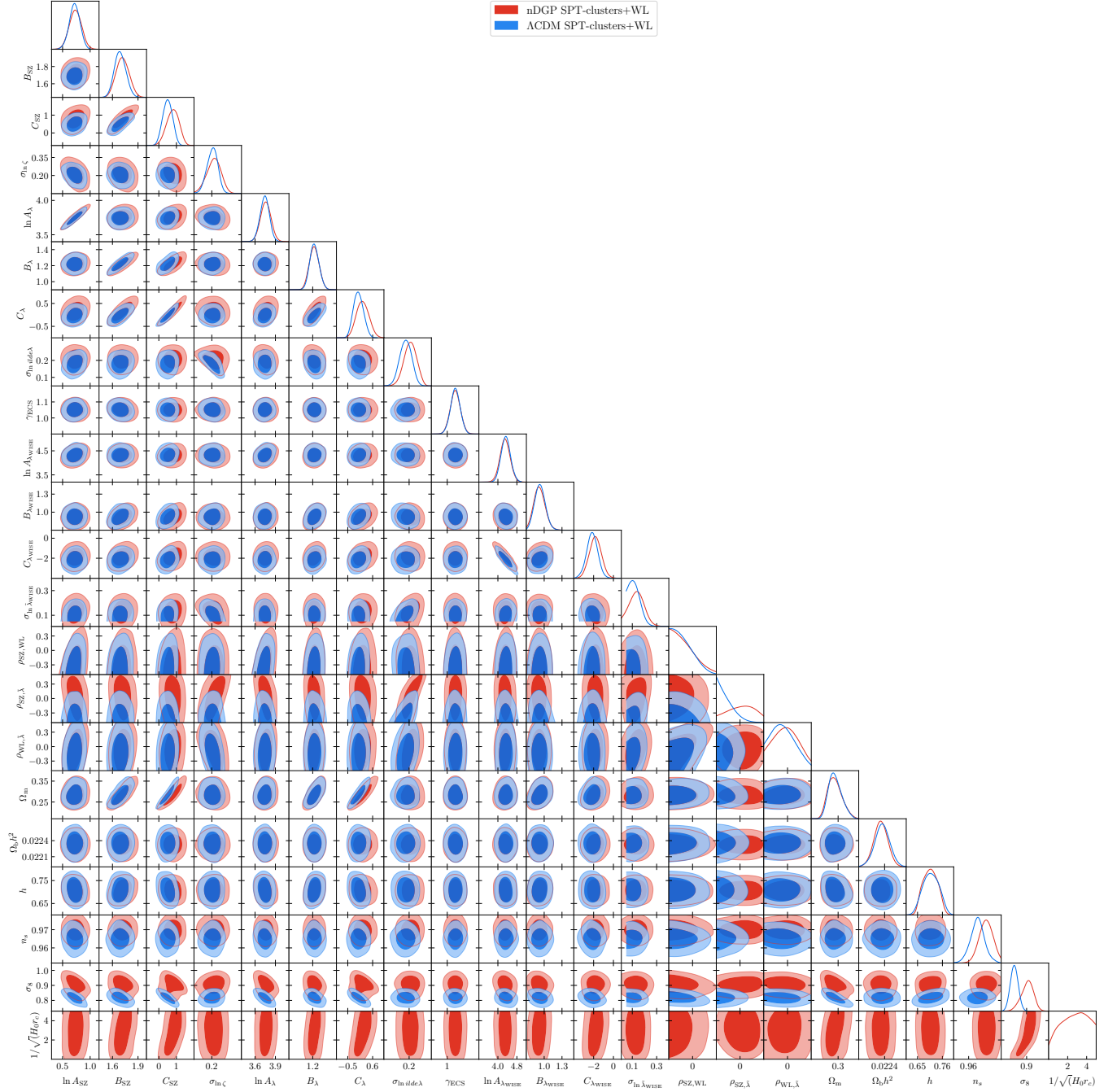


FIG. 6. Posterior distribution for all (non prior dominated) parameters in the SPT-cluster \times WL analysis in the nDGP and $\nu\Lambda$ CDM analyses (68 % and 95 % credible regions). All scaling relation parameters are consistent between the analysis with wider posteriors from the nDGP analysis due to the extra degree of freedom. Only the constraint of the correlations between tSZ significance and richness changes due to a different scatter model applied to the mean richness–mass scaling relation. The shift in n_s come from the different Planck prior applied to our analysis and the analysis from [SB24b].

- [5] T. Baker, A. Barreira, H. Desmond, P. Ferreira, B. Jain, K. Koyama, B. Li, L. Lombriser, A. Nicola, J. Sakstein, et al., arXiv e-prints arXiv:1908.03430 (2019), [arXiv:1908.03430](#).
- [6] G. Dvali, G. Gabadadze, and M. Porrati, Physics Letters B **485**, 208 (2000), [arXiv:hep-th/0005016](#).
- [7] A. I. Vainshtein, Physics Letters B **39**, 393 (1972).
- [8] F. Schmidt, Phys. Rev. D **80**, 123003 (2009), [arXiv:0910.0235](#).
- [9] L. Wang and P. J. Steinhardt, Astrophys. J. **508**, 483 (1998), [arXiv:astro-ph/9804015](#).
- [10] Z. Haiman, J. J. Mohr, and G. P. Holder, Astrophys. J. **553**, 545 (2001), [arXiv:astro-ph/0002336](#).

- [11] A. Vikhlinin, A. V. Kravtsov, R. A. Burenin, H. Ebeling, W. R. Forman, A. Hornstrup, C. Jones, S. S. Murray, D. Nagai, H. Quintana, et al., *Astrophys. J.* **692**, 1060 (2009), [arXiv:0812.2720](#).
- [12] B. A. Benson, T. de Haan, J. P. Dudley, C. L. Reichardt, K. A. Aird, K. Andersson, R. Armstrong, M. L. N. Ashby, M. Bautz, M. Bayliss, et al., *Astrophys. J.* **763**, 147 (2013), [arXiv:1112.5435](#).
- [13] S. Bocquet, A. Saro, J. J. Mohr, K. A. Aird, M. L. N. Ashby, M. Bautz, M. Bayliss, G. Bazin, B. A. Benson, L. E. Bleem, et al., *Astrophys. J.* **799**, 214 (2015), [arXiv:1407.2942](#).
- [14] T. de Haan, B. A. Benson, L. E. Bleem, S. W. Allen, D. E. Applegate, M. L. N. Ashby, M. Bautz, M. Bayliss, S. Bocquet, M. Brodwin, et al., *Astrophys. J.* **832**, 95 (2016), [arXiv:1603.06522](#).
- [15] S. Bocquet, J. P. Dietrich, T. Schrabback, L. E. Bleem, M. Klein, S. W. Allen, D. E. Applegate, M. L. N. Ashby, M. Bautz, M. Bayliss, et al., *Astrophys. J.* **878**, 55 (2019), [arXiv:1812.01679](#).
- [16] T. M. C. Abbott, M. Agüena, A. Alarcon, S. Allam, S. Allen, J. Annis, S. Avila, D. Bacon, K. Bechtol, A. Bermeo, et al., *Phys. Rev. D* **102**, 023509 (2020), [arXiv:2002.11124](#).
- [17] I. N. Chiu, M. Klein, J. Mohr, and S. Bocquet, *MNRAS* **522**, 1601 (2023), [arXiv:2207.12429](#).
- [18] S. Bocquet, S. Grandis, L. E. Bleem, M. Klein, J. J. Mohr, T. Schrabback, T. M. C. Abbott, P. A. R. Ade, M. Agüena, A. Alarcon, et al., *Phys. Rev. D* **110**, 083510 (2024), [arXiv:2401.02075](#).
- [19] V. Ghirardini, E. Bulbul, E. Artis, N. Clerc, C. Garrel, S. Grandis, M. Kluge, A. Liu, Y. E. Bahar, F. Balzer, et al., *AnA* **689**, A298 (2024), [arXiv:2402.08458](#).
- [20] F. Schmidt, A. Vikhlinin, and W. Hu, *Phys. Rev. D* **80**, 083505 (2009), [arXiv:0908.2457](#).
- [21] L. Lombriser, A. Slosar, U. Seljak, and W. Hu, *Phys. Rev. D* **85**, 124038 (2012), [arXiv:1003.3009](#).
- [22] M. Cataneo, D. Rapetti, F. Schmidt, A. B. Mantz, S. W. Allen, D. E. Applegate, P. L. Kelly, A. von der Linden, and R. G. Morris, *Phys. Rev. D* **92**, 044009 (2015), [arXiv:1412.0133](#).
- [23] S. Peirone, M. Raveri, M. Viel, S. Borgani, and S. Ansoldi, *Phys. Rev. D* **95**, 023521 (2017), [arXiv:1607.07863](#).
- [24] S. Hagstotz, M. Costanzi, M. Baldi, and J. Weller, *MNRAS* **486**, 3927 (2019), [arXiv:1806.07400](#).
- [25] E. Artis, V. Ghirardini, E. Bulbul, S. Grandis, C. Garrel, N. Clerc, R. Seppi, J. Comparat, M. Cataneo, Y. E. Bahar, et al., *AnA* **691**, A301 (2024), [arXiv:2402.08459](#).
- [26] S. M. L. Vogt, S. Bocquet, C. T. Davies, J. J. Mohr, and F. Schmidt, *Phys. Rev. D* **109**, 123503 (2024), [arXiv:2401.09959](#).
- [27] A. Mazoun, S. Bocquet, J. J. Mohr, M. Garny, H. Rubira, M. Klein, L. E. Bleem, S. Grandis, T. Schrabback, M. Agüena, et al., *Phys. Rev. D* **111**, 083543 (2025), [arXiv:2411.19911](#).
- [28] S. Zeller, E. Artis, E. Bulbul, S. Grandis, V. Ghirardini, A. von der Linden, Y. E. Bahar, F. Balzer, M. Brüggen, I. Chiu, et al., *arXiv e-prints arXiv:2502.03353* (2025), [arXiv:2502.03353](#).
- [29] S. W. Allen, A. E. Evrard, and A. B. Mantz, *ARAA* **49**, 409 (2011), [arXiv:1103.4829](#).
- [30] G. W. Pratt, M. Arnaud, A. Biviano, D. Eckert, S. Ettori, D. Nagai, N. Okabe, and T. H. Reiprich, *SSR* **215**, 25 (2019), [arXiv:1902.10837](#).
- [31] J. E. Carlstrom, P. A. R. Ade, K. A. Aird, B. A. Benson, L. E. Bleem, S. Busetti, C. L. Chang, E. Chauvin, H. M. Cho, T. M. Crawford, et al., *PASP* **123**, 568 (2011), [arXiv:0907.4445](#).
- [32] R. A. Sunyaev and Y. B. Zeldovich, *Comments on Astrophysics and Space Physics* **4**, 173 (1972).
- [33] M. Klein, J. J. Mohr, S. Desai, H. Israel, S. Allam, A. Benoit-Lévy, D. Brooks, E. Buckley-Geer, A. Carnero Rosell, M. Carrasco Kind, et al., *MNRAS* **474**, 3324 (2018), [arXiv:1706.06577](#).
- [34] M. Klein, J. J. Mohr, S. Bocquet, M. Agüena, S. W. Allen, O. Alves, B. Ansarinejad, M. L. N. Ashby, D. Bacon, M. Bayliss, et al., *MNRAS* **531**, 3973 (2024).
- [35] L. E. Bleem, M. Klein, T. M. C. Abbot, P. A. R. Ade, M. Agüena, O. Alves, A. J. Anderson, F. Andrade-Oliveira, B. Ansarinejad, M. Archipley, et al., *The Open Journal of Astrophysics* **7**, 13 (2024), [arXiv:2311.07512](#).
- [36] B. Flaugher, H. T. Diehl, K. Honscheid, T. M. C. Abbott, O. Alvarez, R. Angstadt, J. T. Annis, M. Antonik, O. Ballester, L. Beaufore, et al., *ApJ* **150**, 150 (2015), [arXiv:1504.02900](#).
- [37] Dark Energy Survey Collaboration, T. Abbott, F. B. Abdalla, J. Aleksić, S. Allam, A. Amara, D. Bacon, E. Balbinot, M. Banerji, K. Bechtol, et al., *MNRAS* **460**, 1270 (2016), [arXiv:1601.00329](#).
- [38] T. M. C. Abbott and et al., *ApJ* **239**, 18 (2018), [arXiv:1801.03181](#).
- [39] E. L. Wright, P. R. M. Eisenhardt, A. K. Mainzer, M. E. Ressler, R. M. Cutri, T. Jarrett, J. D. Kirkpatrick, D. Padgett, R. S. McMillan, M. Skrutskie, et al., *ApJ* **140**, 1868 (2010), [arXiv:1008.0031](#).
- [40] M. Gatti, G. Giannini, G. M. Bernstein, A. Alarcon, J. Myles, A. Amon, R. Cawthon, M. Troxel, J. DeRose, S. Everett, et al., *MNRAS* **510**, 1223 (2022), [arXiv:2012.08569](#).
- [41] T. Schrabback, D. Applegate, J. P. Dietrich, H. Hoekstra, S. Bocquet, A. H. Gonzalez, A. von der Linden, M. McDonald, C. B. Morrison, S. F. Raihan, et al., *MNRAS* **474**, 2635 (2018), [arXiv:1611.03866](#).
- [42] T. Schrabback, S. Bocquet, M. Sommer, H. Zohren, J. L. van den Busch, B. Hernández-Martín, H. Hoekstra, S. F. Raihan, M. Schirmer, D. Applegate, et al., *MNRAS* **505**, 3923 (2021), [arXiv:2009.07591](#).
- [43] H. Zohren, T. Schrabback, S. Bocquet, M. Sommer, F. Raihan, B. Hernández-Martín, O. Marggraf, B. Ansarinejad, M. B. Bayliss, L. E. Bleem, et al., *AnA* **668**, A18 (2022), [arXiv:2208.10232](#).
- [44] S. Bocquet, S. Grandis, L. E. Bleem, M. Klein, J. J. Mohr, M. Agüena, A. Alarcon, S. Allam, S. W. Allen, O. Alves, et al., *Phys. Rev. D* **110**, 083509 (2024), [arXiv:2310.12213](#).
- [45] J. Harnois-Déraps, C. Hernandez-Aguayo, C. Cuesta-Lazaro, C. Arnold, B. Li, C. T. Davies, and Y.-C. Cai, *MNRAS* **525**, 6336 (2023), [arXiv:2211.05779](#).
- [46] C.-Z. Ruan, C. Cuesta-Lazaro, A. Eggemeier, B. Li, C. M. Baugh, C. Arnold, S. Bose, C. Hernández-Aguayo, P. Zarrouk, and C. T. Davies, *MNRAS* **527**, 2490 (2024), [arXiv:2301.02970](#).
- [47] C. T. Davies, J. Harnois-Déraps, B. Li, B. Giblin, C. Hernández-Aguayo, and E. Paillas, *MNRAS* **533**, 3546 (2024), [arXiv:2406.11958](#).
- [48] M. Tristram, A. J. Banday, M. Douspis, X. Garrido, K. M. Górski, S. Henrot-Versillé, L. T. Hergt, S. Ilić, R. Keskitalo, G. Lagache, et al., *AnA* **682**, A37 (2024),

- arXiv:2309.10034.
- [49] A. Barreira, A. G. Sánchez, and F. Schmidt, *Phys. Rev. D* **94**, 084022 (2016), [arXiv:1605.03965](#).
 - [50] L. E. Bleem, B. Stalder, T. de Haan, K. A. Aird, S. W. Allen, D. E. Applegate, M. L. N. Ashby, M. Bautz, M. Bayliss, B. A. Benson, et al., *ApJ* **216**, 27 (2015), [arXiv:1409.0850](#).
 - [51] L. E. Bleem, S. Bocquet, B. Stalder, M. D. Gladders, P. A. R. Ade, S. W. Allen, A. J. Anderson, J. Annis, M. L. N. Ashby, J. E. Austermann, et al., *ApJ* **247**, 25 (2020), [arXiv:1910.04121](#).
 - [52] S. F. Raihan, T. Schrabback, H. Hildebrandt, D. Applegate, and G. Mahler, *MNRAS* **497**, 1404 (2020), [arXiv:2007.01211](#).
 - [53] B. Hernández-Martín, T. Schrabback, H. Hoekstra, N. Martinet, J. Hlavacek-Larrondo, L. E. Bleem, M. D. Gladders, B. Stalder, A. A. Stark, and M. Bayliss, *AnA* **640**, A117 (2020), [arXiv:2007.00386](#).
 - [54] M. W. Sommer, T. Schrabback, D. E. Applegate, S. Hilbert, B. Ansarinejad, B. Floyd, and S. Grandis, *MNRAS* **509**, 1127 (2022), [arXiv:2105.08027](#).
 - [55] S. Shandera, A. Mantz, D. Rapetti, and S. W. Allen, *JCAP* **2013**, 004 (2013), [arXiv:1304.1216](#).
 - [56] L. Lombriser, W. Hu, W. Fang, and U. Seljak, *Phys. Rev. D* **80**, 063536 (2009), [arXiv:0905.1112](#).
 - [57] M. A. Luty, M. Porrati, and R. Rattazzi, *Journal of High Energy Physics* **2003**, 029 (2003), [arXiv:hep-th/0303116](#).
 - [58] A. Nicolis and R. Rattazzi, *Journal of High Energy Physics* **2004**, 059 (2004), [arXiv:hep-th/0404159](#).
 - [59] K. Koyama, *Classical and Quantum Gravity* **24**, R231 (2007), [arXiv:0709.2399](#).
 - [60] W. Fang, S. Wang, W. Hu, Z. Haiman, L. Hui, and M. May, *Phys. Rev. D* **78**, 103509 (2008), [arXiv:0808.2208](#).
 - [61] F. Schmidt, W. Hu, and M. Lima, *Phys. Rev. D* **81**, 063005 (2010), [arXiv:0911.5178](#).
 - [62] M. Wyman and J. Khoury, *Phys. Rev. D* **82**, 044032 (2010), [arXiv:1004.2046](#).
 - [63] L. Xu, *JCAP* **2014**, 048 (2014), [arXiv:1312.4679](#).
 - [64] C. M. Will, *Living Reviews in Relativity* **17**, 4 (2014), [arXiv:1403.7377](#).
 - [65] C. Burrage and J. Sakstein, *Living Reviews in Relativity* **21**, 1 (2018), [arXiv:1709.09071](#).
 - [66] H. Fischer, C. Käding, and M. Pitschmann, *Universe* **10**, 297 (2024), [arXiv:2405.14638](#).
 - [67] R. K. Sheth and G. Tormen, *MNRAS* **308**, 119 (1999), [arXiv:astro-ph/9901122](#).
 - [68] J. Tinker, A. V. Kravtsov, A. Klypin, K. Abazajian, M. Warren, G. Yepes, S. Gottlöber, and D. E. Holz, *Astrophys. J.* **688**, 709 (2008), [arXiv:0803.2706](#).
 - [69] K. Ichiki and M. Takada, *Phys. Rev. D* **85**, 063521 (2012), [arXiv:1108.4688](#).
 - [70] M. Costanzi, F. Villaescusa-Navarro, M. Viel, J.-Q. Xia, S. Borgani, E. Castorina, and E. Sefusatti, *JCAP* **2013**, 012 (2013), [arXiv:1311.1514](#).
 - [71] S. M. L. Vogt, S. Bocquet, C. T. Davies, J. J. Mohr, F. Schmidt, C. Z. Ruan, B. Li, C. Hernández-Aguayo, S. Grandis, L. E. Bleem, et al., *Phys. Rev. D* **111**, 043519 (2025), [arXiv:2409.13556](#).
 - [72] N. Kaiser, *MNRAS* **222**, 323 (1986).
 - [73] R. E. Angulo, V. Springel, S. D. M. White, A. Jenkins, C. M. Baugh, and C. S. Frenk, *MNRAS* **426**, 2046 (2012), [arXiv:1203.3216](#).
 - [74] K. Vanderlinde, T. M. Crawford, T. de Haan, J. P. Dudley, L. Shaw, P. A. R. Ade, K. A. Aird, B. A. Benson, L. E. Bleem, M. Brodwin, et al., *Astrophys. J.* **722**, 1180 (2010), [arXiv:1003.0003](#).
 - [75] F. Schmidt, *Phys. Rev. D* **81**, 103002 (2010), [arXiv:1003.0409](#).
 - [76] J. F. Navarro, C. S. Frenk, and S. D. M. White, *Astrophys. J.* **490**, 493 (1997), [arXiv:astro-ph/9611107](#).
 - [77] M. Bartelmann and M. Maturi, *Scholarpedia* **12**, 32440 (2017), [arXiv:1612.06535](#).
 - [78] M. R. Becker and A. V. Kravtsov, *Astrophys. J.* **740**, 25 (2011), [arXiv:1011.1681](#).
 - [79] M. Oguri and T. Hamana, *MNRAS* **414**, 1851 (2011), [arXiv:1101.0650](#).
 - [80] S. Grandis, S. Bocquet, J. J. Mohr, M. Klein, and K. Dolag, *MNRAS* **507**, 5671 (2021), [arXiv:2103.16212](#).
 - [81] Planck Collaboration, N. Aghanim, Y. Akrami, M. Ashdown, J. Aumont, C. Baccigalupi, M. Ballardini, A. J. Banday, R. B. Barreiro, N. Bartolo, et al., *AnA* **641**, A6 (2020), [arXiv:1807.06209](#).
 - [82] G.-B. Zhao, L. Pogosian, A. Silvestri, and J. Zylberberg, *Phys. Rev. D* **79**, 083513 (2009), [arXiv:0809.3791](#).
 - [83] A. Hojjati, L. Pogosian, and G.-B. Zhao, *JCAP* **2011**, 005 (2011), [arXiv:1106.4543](#).
 - [84] A. Zucca, L. Pogosian, A. Silvestri, and G. B. Zhao, *JCAP* **2019**, 001 (2019), [arXiv:1901.05956](#).
 - [85] Z. Wang, S. H. Mirpoorian, L. Pogosian, A. Silvestri, and G.-B. Zhao, *JCAP* **2023**, 038 (2023), [arXiv:2305.05667](#).
 - [86] M. Ishak, J. Pan, R. Calderon, K. Lodha, G. Valogiannis, A. Aviles, G. Niz, L. Yi, C. Zheng, C. Garcia-Quintero, et al., *JCAP* **2025**, 053 (2025), [arXiv:2411.12026](#).
 - [87] E. Specogna, W. Giarè, and E. Di Valentino, *Phys. Rev. D* **111**, 103510 (2025), [arXiv:2411.03896](#).
 - [88] Planck Collaboration, P. A. R. Ade, N. Aghanim, M. Arnaud, M. Ashdown, J. Aumont, C. Baccigalupi, A. J. Banday, R. B. Barreiro, N. Bartolo, et al., *AnA* **594**, A14 (2016), [arXiv:1502.01590](#).
 - [89] E. Calabrese, A. Slosar, A. Melchiorri, G. F. Smoot, and O. Zahn, *Phys. Rev. D* **77**, 123531 (2008), [arXiv:0803.2309](#).
 - [90] A. Renzi, Ph.D. thesis, SISSA, International School for Advanced Studies, Italy (2013).
 - [91] R. Mokeddem, W. S. Hipólito-Ricaldi, and A. Bernui, *JCAP* **2023**, 017 (2023), [arXiv:2209.11660](#).
 - [92] Planck Collaboration, P. A. R. Ade, N. Aghanim, M. Arnaud, M. Ashdown, J. Aumont, C. Baccigalupi, A. J. Banday, R. B. Barreiro, N. Bartolo, et al., *AnA* **594**, A14 (2016), [arXiv:1502.01590](#).
 - [93] B. A. Benson, P. A. R. Ade, Z. Ahmed, S. W. Allen, K. Arnold, J. E. Austermann, A. N. Bender, L. E. Bleem, J. E. Carlstrom, C. L. Chang, et al., **9153**, 91531P (2014), [arXiv:1407.2973](#).
 - [94] P. Ade, J. Aguirre, Z. Ahmed, S. Aiola, A. Ali, D. Alonso, M. A. Alvarez, K. Arnold, P. Ashton, J. Austermann, et al., *JCAP* **2019**, 056 (2019), [arXiv:1808.07445](#).
 - [95] A. Raccanelli, D. Bertacca, D. Pietrobon, F. Schmidt, L. Samushia, N. Bartolo, O. Doré, S. Matarrese, and W. J. Percival, *MNRAS* **436**, 89 (2013), [arXiv:1207.0500](#).
 - [96] R. Laureijs, J. Amiaux, S. Arduini, J. L. Auguères, J. Brinchmann, R. Cole, M. Cropper, C. Dabin, L. Duvet, A. Ealet, et al., *arXiv e-prints arXiv:1110.3193* (2011), [arXiv:1110.3193](#).
 - [97] LSST Science Collaboration, P. A. Abell, J. Allison, S. F. Anderson, J. R. Andrew, J. R. P. Angel, L. Armus, D. Ar-

- nett, S. J. Asztalos, T. S. Axelrod, et al., arXiv e-prints arXiv:0912.0201 (2009), [arXiv:0912.0201](#).
- [98] E. Camphuis, W. Quan, L. Balkenhol, A. R. Khalife, F. Ge, F. Guidi, N. Huang, G. P. Lynch, Y. Omori, C. Trendafilova, et al., arXiv e-prints arXiv:2506.20707 (2025), [arXiv:2506.20707](#).
- [99] T. Louis, A. La Posta, Z. Atkins, H. T. Jense, I. Abril-Cabezas, G. E. Addison, P. A. R. Ade, S. Aiola, T. Alford, D. Alonso, et al., JCAP **2025**, 062 (2025), [arXiv:2503.14452](#).